Physics and Imaging in Radiation Oncology 28 (2023) 100505

Contents lists available at ScienceDirect

Physics and Imaging in Radiation Oncology

journal homepage: www.sciencedirect.com/journal/physics-and-imaging-in-radiation-oncology

Original Research Article

Accurate, repeatable, and geometrically precise diffusion-weighted imaging on a 0.35 T magnetic resonance imaging-guided linear accelerator

Joseph Weygand [a,*], Tess Armstrong [b], John Michael Bryant [a], Jacqueline M. Andreozzi [a], Ibrahim M. Oraiqat [a], Steven Nichols [a], Casey L. Liveringhouse [a], Kujtim Latifi [a], Kosj Yamoah [a], James R. Costello [c], Jessica M. Frakes [a], Eduardo G. Moros [a], Issam M. El Naqa [a,d], Arash O. Naghavi [a], Stephen A. Rosenberg [a,1], Gage Redler [a,1]

[a] Department of Radiation Oncology, Moffitt Cancer Center, Tampa, FL, USA
[b] ViewRay Inc., Cleveland, OH, USA
[c] Department of Radiology, Moffitt Cancer Center, Tampa, FL, USA
[d] Department of Machine Learning, Moffitt Cancer Center, Tampa, FL, USA

ARTICLE INFO

Keywords:
Diffusion weighted imaging
Apparent diffusion coefficient
Cellularity
MRI-guided radiotherapy

ABSTRACT

Background and purpose: Diffusion weighted imaging (DWI) allows for the interrogation of tissue cellularity, which is a surrogate for cellular proliferation. Previous attempts to incorporate DWI into the workflow of a 0.35 T MR-linac (MRL) have lacked quantitative accuracy. In this study, accuracy, repeatability, and geometric precision of apparent diffusion coefficient (ADC) maps produced using an echo planar imaging (EPI)-based DWI protocol on the MRL system is illustrated, and *in vivo* potential for longitudinal patient imaging is demonstrated.
Materials and methods: Accuracy and repeatability were assessed by measuring ADC values in a diffusion phantom at three timepoints and comparing to reference ADC values. System-dependent geometric distortion was quantified by measuring the distance between 93 pairs of phantom features on ADC maps acquired on a 0.35 T MRL and a 3.0 T diagnostic scanner and comparing to spatially precise CT images. Additionally, for five sarcoma patients receiving radiotherapy on the MRL, same-day *in vivo* ADC maps were acquired on both systems, one of which at multiple timepoints.
Results: Phantom ADC quantification was accurate on the 0.35 T MRL with significant discrepancies only seen at high ADC. Average geometric distortions were 0.35 (±0.02) mm and 0.85 (±0.02) mm in the central slice and 0.66 (±0.04) mm and 2.14 (±0.07) mm at 5.4 cm off-center for the MRL and diagnostic system, respectively. In the sarcoma patients, a mean pretreatment ADC of 910×10^{-6} ($\pm 100 \times 10^{-6}$) mm^2/s was measured on the MRL.
Conclusions: The acquisition of accurate, repeatable, and geometrically precise ADC maps is possible at 0.35 T with an EPI approach.

1. Introduction

Online magnetic resonance imaging-guided radiotherapy (MRgRT) has experienced widespread clinical implementation with two commercially-available fully-integrated MRgRT systems [1,2]. Its primary advantage over other online imaging systems is superior soft-tissue contrast [3] allowing visualization of interfractional/intrafractional changes in size/shape of tumors and surrounding critical structures [4]. This facilitates online adaptive radiotherapy incorporating updated anatomy and daily plan reoptimization [5]. Although MRgRT-driven adaptation based on morphological changes has proven successful [6], MRI's functional imaging capabilities to interrogate tumor physiology *in vivo* [7–9] have not been fully exploited [10].

One physiological parameter accessible by MRI is tumor cellularity [11], which quantifies cellular density within a tumor [12] and is a surrogate for cellular proliferation [13]. Diffusion weighted imaging (DWI), which measures water molecule Brownian motion [14,15] by applying diffusion-sensitizing gradient magnetic fields and observing signal reduction caused by molecular random thermal fluctuations [16], can measure cellularity. Varying diffusion weighting (via b-values [17])

* Corresponding author at: Department of Radiation Oncology, Moffitt Cancer Center, 12902 USF Magnolia Drive, Tampa FL, USA.
E-mail address: joeweygand@gmail.com (J. Weygand).
[1] These authors share senior authorship.

https://doi.org/10.1016/j.phro.2023.100505
Received 24 August 2023; Received in revised form 4 October 2023; Accepted 30 October 2023
Available online 8 November 2023

and modeling exponential signal reduction provides an apparent diffusion coefficient (ADC) [18]. ADC is an important imaging biomarker [19,20], as tumor ADC increases correlate with radiotherapeutic response [21–25] and can be prognostic [26–29] across many disease sites, often preceding morphological signals [30]. Thus, ADC maps have potential in adaptive radiotherapy [31], by allowing identification of cellular subpopulations with restricted diffusion and, hence, increased cellularity [32], for which dose escalation and/or biologically-guided plan adaptation may be clinically advantageous.

Feasibility of DWI on a 0.35 T tri-cobalt MRgRT system has been demonstrated [33,34]. This was illustrated in soft-tissue sarcoma where DWI signal predicted tumor histology [35]. Additionally, DWI combined with deep-learning predicted sarcoma radiotherapeutic response [36]. DWI on a 0.35 T radiotherapy system became more challenging when the tri-cobalt system was replaced by a gantry-mounted linear accelerator (linac) [37]. Eddy currents from the gantry lead to geometric distortion and/or artifacts [38] and can be particularly problematic in echo planar imaging (EPI)-based DWI [39]. It was recently shown that ADC quantification and geometric accuracy on a 0.35 MRI-guided linac (MRL) depended on gantry angle and was markedly inferior to ADC quantification on higher-field diagnostic systems [40]. Moreover, since lower magnetic field has reduced signal-to-noise ratio (SNR) [41], sensitivity concerns, particularly at higher b-values, called into question the feasibility of reliable ADC mapping since noisy data affects accuracy/repeatability of the exponential fit [42].

In this work, ADC maps of a National Institute of Standards and Technology (NIST)-traceable diffusion phantom are acquired on a 0.35 T MRL using single-shot EPI-based [43] diffusion. These are tested for quantitative accuracy over a range of clinically-relevant ADC values and repeatability over multiple measurements, with results compared to those obtained on a 3.0 T diagnostic scanner. Additionally, geometric precision is interrogated via comparison to spatially precise computed tomography (CT) scans of the same phantom. The *in vivo* longitudinal potential of this protocol is illustrated in five patients with soft-tissue sarcoma treated on the MRL and receiving same-day diagnostic DWI scans at one or more timepoints in the patients' treatments.

2. Materials and Methods

2.1. Phantom preparation

A NIST-traceable diffusion phantom (CaliberMRI, Boulder, CO) was imaged. This phantom is a water-filled sphere of radius 9.7 cm and contains thirteen 30-mL cylindrical (2.9 cm inner diameter, 5.0 cm height) vials with varying concentration of polyvinylpyrrolidone (PVP) from 0 to 50 % in 10 % increments. Varying PVP concentration systematically varies ADC. A schematic illustrating the vial PVP concentrations and arrangement within the phantom is in Fig. 1A. With known temperature, NIST-traceable reference ADC can be deduced for comparison to measured ADC. Three phantom measurements were performed on a 0.35 T MRL on different days over three months (constant temperature 22.0° C). Three additional phantom measurements were provided by the phantom vendor for a 3.0 T diagnostic scanner on different days (constant temperature 19.5° C).

2.2. Image acquisition and ADC calculation

Images were acquired on a 0.35 T ViewRay (Oakwood Village OH, USA) MRIdian MRL with gantry at 0° and couch electronics disabled to minimize deleterious RF noise/interference. A pair of 6-channel phased-array receive surface body coils [44] were used for all phantom and patient imaging. A multi-slice EPI diffusion sequence was applied (matrix size = 100x100x21, FOV = 350x350x190 mm^3, 6 mm slice thickness, 3 mm slice gap, TR = 3200 ms, TE = 120 ms, BW = 1352 Hz, α = 90°, 6 averages). GRAPPA-based parallel imaging [45] with an acceleration factor of two was applied to accelerate acquisition and reduce geometric distortions by shortening the echo train [46]. Acquisition took 4.32 min. Phase encoding was anterior-posterior (assuming head-first supine). The b-values were 0, 200, 300, 500, and 800 s/mm^2 with diffusion weighting applied along three principal directions. For a given diffusion direction, voxel ADC was calculated via exponential fit (MATLAB vR2021a, MathWorks, Inc, Natwick MA, USA) as in Equation (1).

$$S(b) = S_0 e^{-bD} \quad (1)$$

S(b) is a voxel signal intensity at b-value b. S_0 is voxel signal intensity at b-value b = 0. D is ADC value. This was applied along each principal direction and average ADC value over each direction in a voxel gave mean diffusivity.

In vivo diffusion images were also acquired using a 3.0 T MAGNETOM Vida (Siemens Healthineers, Erlangen, Germany) diagnostic scanner for comparison to MRL images. A multi-slice EPI diffusion sequence was used (matrix size = 120x120x52, FOV = 280x280x190 mm^3, 3.0 mm slice thickness, 0.75 mm slice gap, TR = 12600 ms, TE = 63 ms, BW = 1603 Hz, α = 90°, 2 averages, 2.23-minute acquisition).

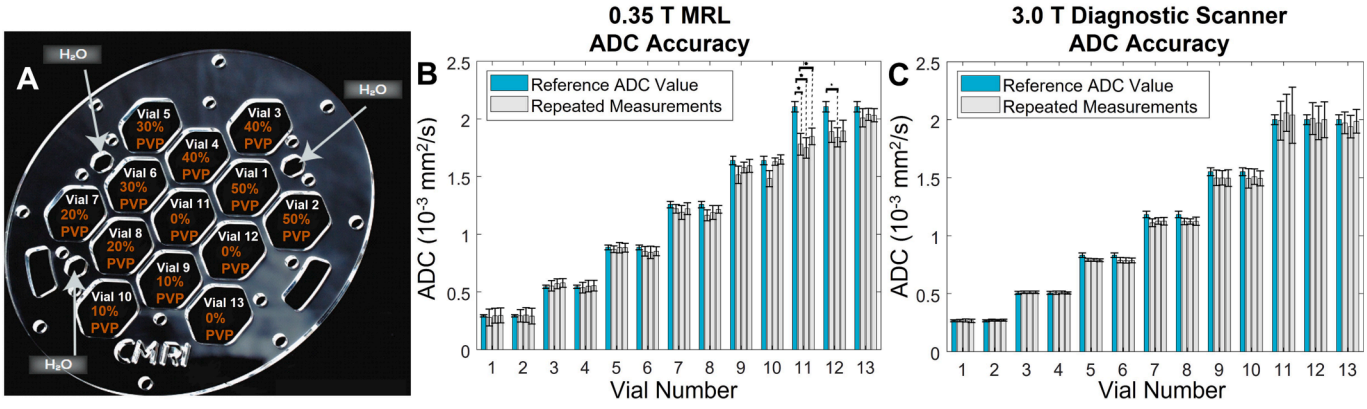

Fig. 1. The accuracy and repeatability of ADC quantification performed on a 0.35 T MRL is depicted and compared to the performance of a 3.0 T diagnostic scanner. 1.A shows a schematic for the diffusion phantom used which contains thirteen vials of differing concentrations of PVP. 1.B demonstrates the measured values of ADC in each vial over three separate measurements (gray) compared to the reference ADC (cyan) in the relevant vial. Here, ADC quantification is accurate and repeatable with significant discrepancies (as denoted by a star) only seen in vials approaching free diffusion where the SNR is low. Similarly, the accuracy and repeatability of ADC mapping on a typical 3.0 T diagnostic scanner is shown in 1.C. Standard deviations of the measured values reflect the variation in ADC over each voxel in a given vial. Standard deviations of the reference values were provided by the phantom manufacturer. (For interpretation of the references to colour in this figure legend, the reader is referred to the web version of this article.)

Two-fold GRAPPA was applied. This clinical protocol utilizes b-values of 100 and 1000 s/mm^2 with diffusion weighting applied along a single direction (as opposed to all three principal directions). Equation (1) was applied unidirectionally to calculate ADC.

2.3. ADC accuracy and repeatability measurement in phantom

Three repeated scans were acquired on both the 0.35 T MRL and a 3.0 T diagnostic scanner. ADC was determined in each voxel using Equation (1), as described above. Mean ADC for a cylindrical (2.1 cm diameter, 2.7 cm height) region of interest (ROI) centered within each vial was calculated. Mean and standard deviation (σ) of mean vial ADC over repeat experiments were calculated and compared to known NIST-traceable values (provided for given temperature with associated uncertainty by vendor). A two-tailed *t*-test (MATLAB) between measured vial ADC values over the three experiments and corresponding reference ADC values was used. A measurement was deemed significantly different from expected value when $p < 0.05$.

The repeatability coefficient (RC) assessing agreement between repeated measurements, was quantified as [47]

$$RC = 2.77\sigma \quad (2)$$

RC was calculated for each vial and averaged across all thirteen vials (mean RC) for both 0.35 T and 3.0 T.

2.4. Geometric distortion analysis

Phantom CT images were acquired on a Philips (Amsterdam, Netherlands) Brilliance 64 scanner in axial-mode (matrix size = 512x512x160, FOV = 240x240x270 mm^3, 1.25 mm slice thickness) and taken as geometric ground truth for comparing phantom ADC maps produced from diffusion images acquired on both the 0.35 T MRL and the 3.0 T diagnostic scanner. Nineteen structures were separately contoured by three independent observers (RayStation v11A, RaySearch Laboratories, Stockholm, Sweden) on CT and both ADC maps: thirteen vials in the central slice (Fig. 2A-C) and six plastic screws 5.4 cm from the central slice (Fig. 2D-F). The distances between the geometric center for 78 vial pairs (central slice) and fifteen screw pairs (5.4 cm off-center) were determined. System-dependent geometric distortion was quantified as the difference in distance between a given pair of structures measured from an ADC map relative to the CT image [48]. Mean geometric distortion for each observer was calculated by averaging over all structures in each slice. A one-tailed *t*-test (MATLAB) determined geometric distortion statistical significance (0.35 T less than 3.0 T geometric distortion if $p < 0.05$)), both in the central and 5.4 cm off-center slices. The slice 5.4 cm off-center was chosen for its discernible phantom features. Mean geometric distortion standard deviation taken over the three observers provided a measure of uncertainty for this geometric distortion quantification.

2.5. Sarcoma imaging

DWI was performed on five patients with high-grade soft-tissue sarcoma of the thigh on the institutional review board (IRB)-approved Habitat Escalated Adaptive Therapy (HEAT) protocol (NCT05301283), a phase 2 clinical trial utilizing functional imaging-defined habitats to identify radioresistant tumor subpopulations. Imaging was in treatment position, with one patient imaged at three timepoints: pre-treatment simulation (day 0), mid-treatment (day 21), and three weeks post-treatment (day 69). The other four patients were imaged during simulation (pre-treatment) only. For all patients/timepoints, same-day diffusion-weighted imaging was performed on a 3.0 T diagnostic scanner. MRL anatomical imaging used a balanced steady-state free precession (bSSFP) sequence [49,50]. The gross tumor volume (GTV) was delineated by a radiation oncologist on the bSSFP images. The ADC maps (MRL and diagnostic) were rigidly registered to anatomical images (Mirada Medical, Oxford, UK). Mean ADC within the GTV was determined for each image. The mean and standard deviation of the mean ADC values across the five patients was determined.

3. Results

Phantom ADC quantification was accurate on the 0.35 T MRL for clinically relevant ADC values, with discrepancies beyond measurement uncertainty only in vials approaching free diffusion (Fig. 1B). Three measurements at different times are in gray and compared to reference ADC (cyan). Phantom ADC measurements at 0.35 T are in Table 1. Four of thirty-nine measurements (thirteen vials, three repetitions) on the 0.35 T MRL deviated significantly (asterisk in Fig. 1B) from reference ADC. These were all three measurements in vial 11 ($p = 0.026$, 0.020, and 0.029) and one measurement in vial 12 ($p = 0.032$). Both vials have 0 % PVP concentration and high ADC, which is expected to have diminished accuracy [51] due to lower SNR (increased signal loss due to greater diffusion). The other thirty-five measurements did not deviate significantly from reference ADC. At 3.0 T, ADC quantification was accurate (no significant deviations from reference) across all ADC values

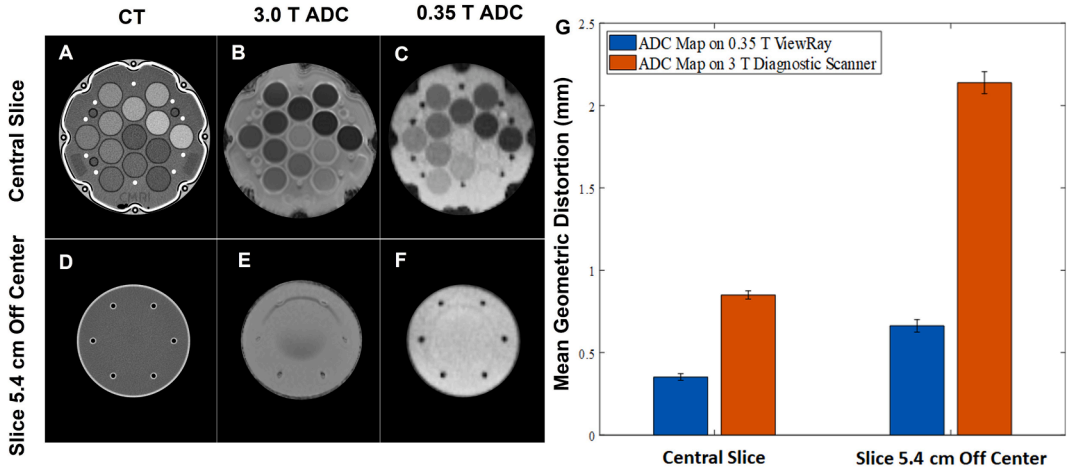

Fig. 2. The geometric accuracy of ADC maps produced on a 0.35 T MRL and 3.0 T diagnostic scanner are compared. The distance between 93 pairs of phantom structures were measured on each system and compared to their distances measured on a CT. Mean geometric accuracy is shown to be superior relative to the 3 T diagnostic scanner and submillimeter on the 0.35 T MRL in both a central slice and a slice that is displaced by 5.4 cm from the central slice. Here, the mean was taken over each of the 93 measurements and over each of the three observers.

Table 1

*All ADC measurements are given in units of 10^{-6} mm^2/s

Vial	PVP Concentration	ADC Measurement 1	ADC Measurement 2	ADC Measurement 3	Reference ADC
1	50 %	278 (±74)	294 (±65)	296 (±65)	293 (±9)
2	50 %	293 (±53)	300 (±64)	291 (±68)	293 (±9)
3	40 %	553 (±45)	571 (±42)	578 (±39)	545 (±14)
4	40 %	553 (±45)	571 (±42)	578 (±39)	545 (±14)
5	30 %	870 (±29)	884 (±45)	883 (±38)	886 (±21)
6	30 %	853 (±41)	844 (±54)	853 (±40)	886 (±21)
7	20 %	1221 (±38)	1190 (±60)	1222 (±52)	1258 (±28)
8	20 %	1165 (±48)	1189 (±59)	1215 (±33)	1258 (±28)
9	10 %	1516 (±76)	1579 (±47)	1593 (±56)	1640 (±36)
10	10 %	1483 (±70)	1630 (±32)	1649 (±40)	1640 (±36)
11	0 %	1781 (±95)	1750 (±89)	1849 (±72)	2106 (±45)
12	0 %	1890 (±93)	1840 (±83)	1897 (±93)	2106 (±45)
13	0 %	2010 (±80)	2040 (±53)	2032 (±58)	2106 (±45)

*All ADC measurements are given in units of 10^{-6} mm^2/s.

(Fig. 1B), likely due to increased SNR at higher field strength. ADC quantification was repeatable on the 0.35 T MRL, with small discrepancies again only seen at high ADC. Mean RC for the 0.35 T MRL versus 3.0 T diagnostic scanner was $68x10^{-6}$ mm^2/s versus $57x10^{-6}$ mm^2/s.

In the central slice, average system-dependent geometric distortions were 0.35 (±0.02) mm and 0.85 (±0.02) mm for the MRL and diagnostic system, respectively (Fig. 2G). In the slice 5.4 cm off-center, these were 0.66 (±0.04) mm and 2.14 (±0.07) mm, respectively (Fig. 2G). 0.35 T MRL ADC maps are significantly more geometrically precise than the 3.0 T ADC maps, in both the central ($p < 0.0001$) and off-center slice ($p < 0.0001$). Geometric distortion can be visualized in Fig. 2A-F.

Longitudinally acquired *in vivo* sarcoma images for both systems provided sufficient image quality to visualize intratumoral spatially-varying ADC features. ADC maps for all three imaging timepoints (axial and coronal planes) for one patient along with MRL anatomical bSSFP images are shown with the radiation oncologist-delineated GTV (Fig. 3) The general region of enhanced ADC on 0.35 T MRL images demonstrates marked conformity with the anatomically derived GTV. Mean GTV ADC measurements of $800x10^{-6}$ ($\pm 450x10^{-6}$) mm^2/s, $1020x10^{-6}$ ($\pm 490x10^{-6}$) mm^2/s, and $820x10^{-6}$ ($\pm 470x10^{-6}$) mm^2/s were obtained for the three timepoints, respectively. Moreover, the general pattern of ADC heterogeneity in the diagnostic ADC maps is qualitatively reproduced in MRL ADC maps. DWI on the MRL is robust to motion, as motion-artifacts in the post-treatment MRL anatomical images are not discernable in resulting MRL ADC maps. However, tumor ADC heterogeneity and anatomical features outside of GTV are less discernible at 0.35 T than at 3.0 T. In five sarcoma patients imaged on the 0.35 T MRL pre-treatment, mean GTV ADC was $910x10^{-6}$ ($\pm 100x10^{-6}$) mm^2/s. MRL anatomical bSSFP images, 3.0 T ADC maps and 0.35 T ADC maps are shown for each patient (Fig. 4).

4. Discussion

In this study, an EPI-based diffusion protocol demonstrated notable improvement in ADC quantification and repeatability. These ADC maps were geometrically precise (submillimeter precision) despite the susceptibility of EPI-based protocols to eddy current-induced geometric distortion. Also, the *in vivo* potential of this technique is illustrated.

To the best of the authors' knowledge, there has been only one previous EPI-based study performing DWI on a 0.35 T MRL. Lewis et al. [40] quantified ADC accuracy as a function of gantry position and assessed geometric distortions. The current study, however, utilizes a new diffusion acquisition protocol and demonstrates a considerable improvement in ADC quantification accuracy. For example, for PVP concentrations providing ADC values in the range $200\text{-}300x10^{-6}$ mm^2/s, Lewis et al. reported minimum ADC deviations from reference of 26.6 %,

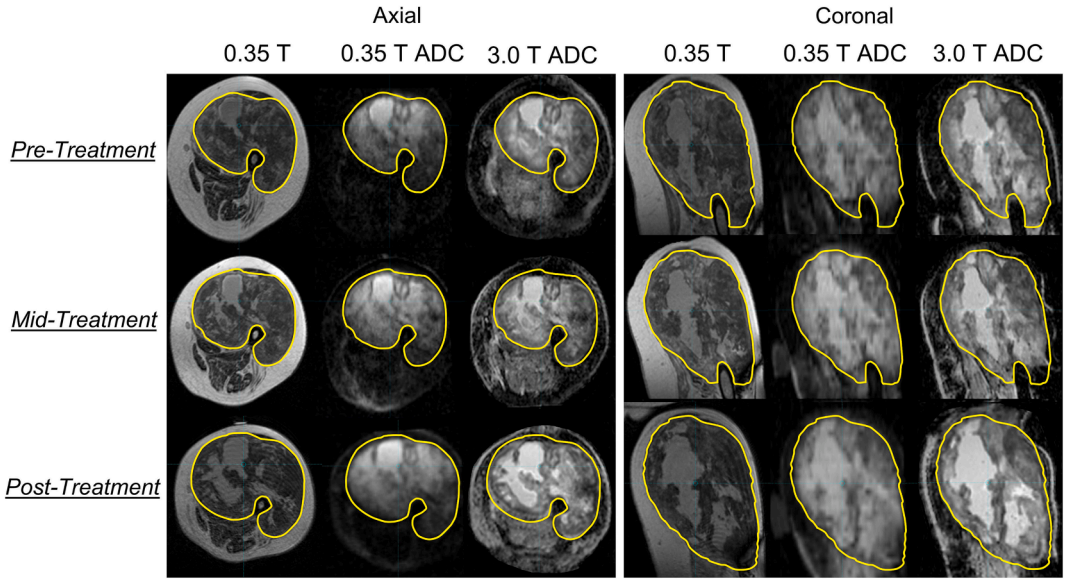

Fig. 3. The feasibility of *in vivo* diffusion imaging on a 0.35 T MRL and its longitudinal potential are illustrated in a sarcoma patient who received same-day diagnostic diffusion scans at three timepoints, shown in axial and sagittal views. The region of enhanced signal in the ADC maps acquired at 0.35 T exhibits notable conformity with the tumor contours delineated on an anatomical bSSFP image (shown in green) and similarity with tumor ADC features seen in the ADC maps acquired at 3 T. (For interpretation of the references to colour in this figure legend, the reader is referred to the web version of this article.)

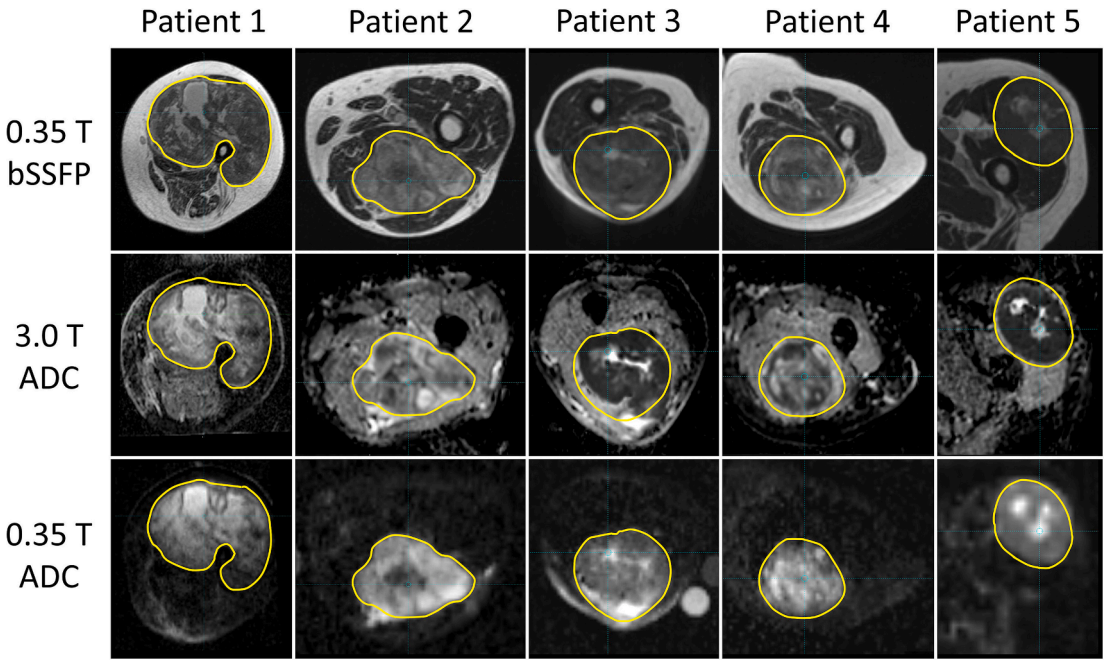

Fig. 4. Five sarcoma patients with disease of the upper thigh are imaged. The top row displays the set of anatomical bSSFP images with the tumor contours delineated in green. The middle row is a set of ADC maps acquired on a 3.0 T diagnostic scanner. The middle row is a set of ADC maps acquired on a 0.35 T MRL on the same day as their corresponding diagnostic ADC map. (For interpretation of the references to colour in this figure legend, the reader is referred to the web version of this article.)

while the current study observed mean ADC deviations from reference of 0.4 %. Similarly, for PVP concentrations providing ADC values in the range 800-900x10^{-6} mm^2/s, Lewis et al. reported minimum ADC deviations from reference of 7.2 %, while the current study observed mean ADC deviations from reference of 2.4 %. Additionally, the current study provides robust geometric distortion assessment with distances between 93 pairs of structures in two planes assessed (three pairs of structures in the central plane were analyzed in Lewis et al. [40]). Specific sequence details were not provided in Lewis et al. to speculate why the current study outperforms their results. The novelty of the current study lies not in the EPI pulse sequence applied, as this is commonly used in DWI, but in that this is the first study to demonstrate accurate/repeatable ADC mapping on a low-field MRL.

Mean ADC across five sarcoma tumors was 910x10^{-6} (±100x10^{-6}) mm^2/s, which in agreement with 1.5 T published values. Oka et al. [52] measured mean ADC of malignant soft-tissue tumors to be 920x10^{-6} (±139x10^{-6}) mm^2/s. In a later study, the same group [53] measured mean malignant soft-tissue tumor ADC of 880x10^{-6} (±200x10^{-6}) mm^2/s. Razek et al. [54] measured malignant soft tissue tumors of extremities mean ADC of 1020x10^{-6} (±300x10^{-6}) mm^2/s.. The analogous value of 910x10^{-6} in this work on a 0.35 T MRL is in agreement, suggesting promising *in vivo* accuracy.

An alternative turbo spin echo (TSE)-based DWI approach [55] on a 0.35 T MRL [56] produced distortion-free ADC maps on the tri-cobalt system. TSE-based approaches suffer less from geometric distortion than EPI-based approaches (multiple 180° refocusing pulses allow less phase accumulation than during the long single-shot EPI echo train [57,58]. However, this TSE-based approach on the MRL was plagued by signal-dropout artifacts [59] that may have been from eddy currents produced by linac gantry electrical components or concomitant gradients (extraneous magnetic gradients produced to satisfy the Ampere-Maxwell equation [60]), but further investigation is necessary to confirm this.

DWI has been performed using a 1.5 T MRL [51,61–63] and may be an option at MR simulation [64]. While the 1.5 T MRL system allows ADC accuracy/repeatability quantification [61] similar to the current study, geometric accuracy results are not reported. The current study demonstrates not only ADC accuracy/repeatability but also submillimeter precision even in objects > 7 cm (Euclidean distance) from isocenter. Although DWI on a 0.35 T MRL is not yet as established as on a 1.5 T MRL, spatial precision dependence on field strength [65] alluded to in this work may indicate an advantage of incorporating DWI on the lower-field MRL system due to the importance of spatial precision in radiotherapy.

In the literature, DWI accuracy at high b-values using a single-shot EPI approach has been controversial due to lower sensitivity at 0.35 T relative to clinical field strengths [55]. Measuring ADC map SNR is nontrivial, since it is derived from exponential fitting. This study addressed this by measuring repeatability [66] of 0.35 T MRL ADC quantification. The introduction of noise diminishes the exponential fit accuracy/stability and, subsequently, results in larger ADC variance over repeated measurements. However, despite having lower sensitivity than the 3.0 T diagnostic system, the 0.35 T MRL repeatability coefficient was only slightly inferior. Thus, sensitivity limitations inherent in operating at 0.35 T do not preclude repeatable ADC measurements.

The current study only assesses system-dependent geometric distortion. Additional distortions are created when introducing a patient into the magnetic field, due to magnetic susceptibility effects [67] and chemical shift [68]. This represents a potential limitation of this study since patient-dependent geometric distortions were not assessed. Both effects scale with magnetic field strength [69,70] and would, thus, be smaller on a lower-field MRL. However, since EPI-based approaches are particularly prone to susceptibility effects [71], patient-dependent geometric distortion in this context should be investigated in future studies. Another limitation of the distortion analysis in this study is that it only measured the centroid-to-centroid distance between structures, which is not sensitive to distortions in object shape.

Another limitation of this study is that b-values are not optimized. Using five b-values along each direction may not increase ADC quantification accuracy, and acquisition duration could be reduced (or SNR increased with more averages) by reducing these measurements. Moreover, lower/upper b-value limits have not been investigated. At

low b-values, the phenomena of diffusion and perfusion become coupled [72], and signal decrease departs from mono-exponential behavior [73]. This is typically observed at b-values less than 100–150 s/mm^2 [74]. This would not manifest in phantom measurements (perfusion not present), but its effect on *in vivo* ADC quantification needs investigation. Optimal maximum b-value should be determined. Consensus recommendations for DWI on the 1.5 T MRL [75] advise against b-values > 500 s/mm^2 due to gradient limitations and sensitivity concerns. While images acquired in the current study using a b-value of 800 s/mm^2 qualitatively looked sufficiently sensitive, a deeper investigation into how lower sensitivity at higher b-values affects ADC quantification is warranted. Other imaging parameters such as echo time, repetition time, voxel size, and bandwidth all still need to be more rigorously optimized for application-specific image quality.

Another limitation of this study is the fact that the imaging parameters for DWI on the 0.35 T MRL and the 3.0 T diagnostic scanner differ. For the latter, routine protocol parameters were used. For the MRL, these parameters were modified due to lower overall sensitivity of the low-field system. For example, a larger slice thickness and lower maximum b-value were used on the MRL because the parameters in the diagnostic scan would result in unacceptable sensitivity reduction. It is not the intent of this manuscript to directly compare the lower-field MRL and higher-field diagnostic system. Instead, it illustrates the feasibility of accurate/repeatable DWI on a 0.35 T MRL while highlighting its advantages (geometric precision, logistics) and disadvantages (sensitivity) relative to the 3.0 T diagnostic system.

It should also be noted that ADC heterogeneity is only discernible within the GTV on the ADC maps acquired at 0.35 T. While this is not entirely understood, it could be due to the fact that the SNR is highest in the tumor because the coils were placed directly adjacent to the tumor for each patient. Further investigation is warranted.

Note, the NIST-traceable ADC values used as reference were specified at a field strength of 3.0 T [76]. However, ADC quantification can change slightly with field strength [77], although other studies are less conclusive [78]. Since 0.35 T is an uncommon field strength, no quantification standards exist for ADC at 0.35 T, making the NIST-traceable values at 3 T a best approximation.

In conclusion, the acquisition of accurate, repeatable, and geometrically precise (sub-millimeter distortion; greater than two-fold improvement over 3.0 T) ADC maps is possible at 0.35 T with an EPI approach. This enables tracking of longitudinal changes in tumor cellular density over the course of treatment on a low-field MRL. This may help facilitate biologically-guided online plan adaptation based upon a tumor's dynamic physiologic changes over the course of treatment.

Author contribution

All authors contributed to the writing and preparation of the manuscript. JW, JA, IMO, SN, KL, and GR participated in the data collection. JW, JMB, and GR analyzed the geometric distortion data. CLL helped with the statistical analyses. TA designed the pulse sequence. JRC and AON designed the diagnostic imaging protocol. JMB, JMF, KY, AON, and SAR provided the clinical perspective for the manuscript. KL, EGM, and IMEN provided the technical perspective for the manuscript. SAR and GR provided the vision for the manuscript from the clinical and technical sides, respectively. JW led the project.

Declaration of competing interest

The authors declare the following financial interests/personal relationships which may be considered as potential competing interests: JW, the first and corresponding author, has nothing to declare. Amongst the coauthors, TA was an employee of ViewRay, Inc at the time this work was performed and owned ViewRay, Inc stocks at that time. EGM, JMF, and SAR have been supported by a grant/contract from ViewRay, Inc. KL and SAR have consulted for ViewRay, Inc.

Acknowledgements

The authors would like to express gratitude to Dr. Vladimir Feygelman of Moffitt Cancer Center and Dr. Hui Wang previously of ViewRay Inc. for their insightful comments during the preparation of this manuscript. This work was partially funded by ViewRay Inc. and partially by an internal Moffitt Cancer Center GME trainee research grant.

References

[1] Raaymakers BW, Lagendijk JJW, Overweg J, Kok JGM, Raaijmakers AJE, Kerkhof EM, et al. Integrating a 1.5 T MRI scanner with a 6 MV accelerator: Proof of concept. Phys Med Biol 2009; 54:N229-N237.
[2] Mutic S, Gempsey JF. The ViewRay system: magnetic resonance–guided and controlled radiotherapy. Semin Radiat Oncol 2014;24:196–9.
[3] Khoo VS, Dearnaley DP, Finnigan DJ, Padhani A, Tanner SF, Leach MO. Magnetic resonance imaging (MRI): Considerations and applications in radiotherapy treatment planning. Radiother Oncol 1997;42:1–15.
[4] De Ridder M, Raaijmakers CPJ, Pameijer FA, De Bree R, Reinders FCJ, Doonaert PAH, et al. Cancers 2022;14:3027.
[5] Acharya S, Fischer-Valuck BW, Kashani R, Parikh P, Yang D, Zhao T, et al. Online magnetic resonance image guided adaptive radiation therapy: First clinical applications. Int J Radiat Oncol Biol Phys 2016;94:394–403.
[6] Thureau S, Briens A, Decazes P, Castelli J, Barateau A, Garcia R, et al. PET and MRI guided adaptive radiotherapy: Rational, feasibility and benefit. Cancer Radiother 2020;24:635–44.
[7] Wang J, Weygand J, Hwang KP, Mohamed ASR, Ding Y, Fuller CD, et al. Magnetic resonance imaging of glucose uptake and metabolism in patients with head and neck cancer. Sci Rep 2016;6:30618.
[8] Dutta P, Perez MR, Lee J, Kang Y, Pratt M, Salzillo TC, et al. Combining hyperpolarized real-time metabolic imaging and NMR spectroscopy to identify metabolic biomarkers in pancreatic cancer. J Proteome Res 2019;18:2826–34.
[9] Salzillo TC, Mawoneke V, Weygand J, Shetty A, Gumin J, Zacharias NM, et al. Measuring the metabolic evolution of glioblastoma throughout tumor development, regression, and recurrence with hyperpolarized magnetic resonance. Cells 2021;10:2621.
[10] Bryant JM, Weygand J, Keit E, Cruz-Chamorro R, Sandoval ML, Oraiqat IM, et al. Stereotactic magnetic resonance-guided adaptive and non-adaptive radiotherapy on combination MR-linear accelerators: Current practice and future directions. Cancers 2023;15:2081.
[11] Sugahara T, Korogi Y, Kochi M, Ikushima I, Shigematu Y, Hirai T, et al. Usefulness of diffusion-weighted MRI with echo-planar technique in the evaluation of cellularity in gliomas. J Magn Reson Imaging 1999;9:53–60.
[12] Rajan R, Poniecka A, Smith TL, Yang Y, Frye D, Pusztai L, et al. Change in tumor cellularity of breast carcinoma after neoadjuvant chemotherapy as a variable in the pathologic assessment of response. Cancer 2004;100:1365–73.
[13] Onishi N, Kanao S, Kataoka M, Iima M, Sakaguchi R, Kawai M, et al. Apparent diffusion coefficient as a potential surrogate marker for Ki-67 index in mucinous breast carcinoma. J Magn Reson Imaging 2015;41:610–5.
[14] Brown R. A brief account of microscopical observations made in the months of June, July and August 1827, on the particles contained in the pollen of plants; and on the general existence of active molecules in organic and inorganic bodies. Phil Mag 1828;4:171–3.
[15] Einstein A. Über die von der molekularkinetischen Theorie der Wärme geforderte Bewegung von in ruhenden Flüssigkeiten suspendierten Teilchen. Ann Phys 1905; 17:649-560.
[16] Le Bihan D, Breton E, Lallemand D, Grenier P, Cabanis E, Laval-Jeantet M. MR imaging of intravoxel incoherent motions: Application to diffusion and perfusion in neurologic disorders. Radiology 1986;161:401–7.
[17] Maier SE, Wallström J, Langkilde F, Johansson J, Kuczera S, Hugosson J, et al. Prostate cancer diffusion-weighted magnetic resonance imaging: Does the choice of diffusion-weighting level matter? J Magn Reson Imaging 2022;55:842–53.
[18] Bammer R. Basic principles of diffusion-weighted imaging. Eur J Radiol 2003;45: 169–84.
[19] Boraschi P, Donati F, Cervelli R, Pacciardi F, Tarantini G, Castagna M, et al. Colorectal liver metastases: ADC as an imaging biomarker of tumor behavior and therapeutic response. Eur J Radiol 2021;137:109609.
[20] Messina C, Bignone R, Bruno A, Bruno A, Bruno F, Calandri M, et al. Diffusion-weighted imaging in cancer: An update. Cancer 2020;12:1493.
[21] Vandecaveye V, Dirix P, De Keyzer F, De Beeck KO, Vander Poorten V, Roebben I, et al. Predictive value of diffusion-weighted magnetic resonance imaging during chemoradiotherapy for head and neck squamous cell carcinoma. Eur Radiol 2010; 20:1703–4.
[22] Chang Q, Wu N, Ouyang H, Huang Y. Diffusion-weighted magnetic resonance imaging of lung cancer at 3.0 T: A preliminary study on monitoring diffusion changes during chemoradiation therapy. Clin Imaging 2012;36:98–103.
[23] Yoshida S, Koga F, Kobayashi S, Ishii C, Tanaka H, Tanaka H, et al. Role of diffusion-weighted magnetic resonance imaging in predicting sensitivity to chemoradiotherapy in muscle-invasive bladder cancer. Int J Radiat Oncol Biol Phys 2012; 83:e21-e27.

[24] Decker G, Mürtz P, Gieseke J, Träber F, Block W, Sprinkart AM, et al. Intensity-modulated radiotherapy of the prostate: dynamic ADC monitoring by DWI at 3.0 T. Radiother Oncol 2014;113:115–20.

[25] Kuang F, Yan Z, Wang J, Rao Z. The value of diffusion-weighted MRI to evaluate the response to radiochemotherapy for cervical cancer. Magn Reson Imaging 2014; 32:342–439.

[26] Jingu K, Kishimoto R, Mizoe JE, Hasegawa A, Bessho H, Tsuji H, et al. Malignant mucosal melanoma treated with carbon ion radiotherapy with concurrent chemotherapy: Prognostic value of pretreatment apparent diffusion coefficient (ADC). Radiother Oncol 2011;98:68–73.

[27] Punwani S, Taylor SA, Saad ZZ, Bainridge A, Groves A, Daw S, et al. Diffusion-weighted MRI of lymphoma: prognostic utility and implications for PET/MRI? Eur J Nucl Med Mol Imaging 2013;30:373–85.

[28] Zhang Y, Liu X, Zhang Y, Li WF, Chen L, Mao YP, et al. Prognostic value of the primary lesion apparent diffusion coefficient (ADC) in nasopharyngeal carcinoma: A retrospective study of 541 cases. Sci Rep 2015;5:1–9.

[29] Kurokawa R, Baba A, Kurokawa M, Capizzano A, Hassan O, Johnson T, et al. Pretreatment ADC histogram analysis as a prognostic imaging biomarker for patients with recurrent glioblastoma treated with bevacizumab: A systematic review and meta-analysis. Am J Neuroradiol 2022;43:202–26.

[30] Bains LJ, Zweifel M, Thoeny HC. Therapy response with diffusion MRI: An update. Cancer Imaging 2012;12:395–402.

[31] Gani C, Boldrini L, Valentini V. Online MR guided radiotherapy for rectal cancer. New opportunities Clin Transl Radiat Oncol 2019;18:66–7.

[32] Akbar S, Peikari M, Salama S, Panah AY, Nofech-Mozes S, Martel AL. Automated and manual quantification of tumour cellularity in digital slides for tumour burden assessment. Sci Rep 2019;9:14099.

[33] Yang Y, Cao M, Sheng K, Gao Y, Chen A, Kamrava M, et al. Longitudinal diffusion MRI for treatment response assessment: Preliminary experience using an MRI-guided tri-cobalt 60 radiotherapy system. Med Phys 2016;43:1369–73.

[34] Shaverdian N, Yang Y, Hu P, Hart S, Sheng K, Lamb J, et al. Feasibility evaluation of diffusion-weighted imaging using an integrated MRI-radiotherapy system for response assessment to neoadjuvant therapy in rectal cancer. Br J Radiol 2017;90: 20160739.

[35] Kalbasi A, Kamrava M, Chu FI, Telesca D, Van Dams R, Yang Y, et al. A phase II trial of 5-day neoadjuvant radiotherapy for patients with high-risk primary soft tissue sarcoma Five-Day Neoadjuvant Radiation for Soft Tissue Sarcoma. Clin Cancer Res 2020;26:1829–36.

[36] Gao Y, Ghodrati V, Kalbasi A, Fu J, Ruan D, Cao M, et al. Prediction of soft tissue sarcoma response to radiotherapy using longitudinal diffusion MRI and a deep neural network with generative adversarial network-based data augmentation. Med Phys 2021;48:3262–72.

[37] Klüter S. Technical design and concept of a 0.35 T MR-Linac. Clin Transl Radiat Oncol 2019;18:98–101.

[38] Gach HM, Curcuru AN, Kim T, Yang D. Effects of rotating gantry on magnetic field and eddy currents in 0.35 T MRI-guided radiotherapy (MR-IGRT) system. Med Phys 2021;48:7228–35.

[39] Spees WM, Buhl N, Sun P, Ackerman JJH, Neil JJ, Garbow JR. Quantification and compensation of eddy-current-induced magnetic-field gradients. J Magn Reson 2011;212:116–23.

[40] Lewis B, Guta A, Mackey S, Gach HM, Mutic S, Green O, et al. Evaluation of diffusion-weighted MRI and geometric distortion on a 0.35 T MR-LINAC at multiple gantry angles. J Appl Clin Med Phys 2021;22:118–25.

[41] Gao Y, Lotey R, Low DA, Hu PP, Yang Y. Technical Note: Validation of an automatic ACR phantom quality assurance tool for an MR-guided radiotherapy system. Med Phys 2021;48:1540–2155.

[42] Saritas EU, Lee JH, Nishimura DG. SNR dependence of optimal parameters for apparent diffusion coefficient measurements. IEEE Trans Med Imaging 2011;30: 424–37.

[43] Mansfield P. Multi-planar imaging formation using NMR spin-echo. J Phys C 1977; 10:L55-L58.

[44] Acharya S, Fischer-Valuck BW, Mazur TR, Curcuru A, Sona K, Kashani R, et al. Magnetic resonance image guided radiation therapy for external beam accelerated partial-breast irradiation: evaluation of delivered dose and intrafractional cavity motion. Int J Radiat Oncol Biol Phys 2016;96:785–92.

[45] Griswold MA, Jakob PM, Heidemann RM, Nittka M, Jellus V, Wang J, et al. Generalized autocalibrating partially parallel acquisitions (GRAPPA). Magn Reson Med 2002;47:1202–10.

[46] Hoge WS, Polimeni JR. Dual-polarity GRAPPA for simultaneous reconstruction and ghost correction of echo planar imaging data. Magn Reson Med 2016;76:32–44.

[47] Obuchowski NA, Reeves AP, Huang EP, Wang XF, Buckler AJ, Kim HJ, et al. Quantitative imaging biomarkers: A review of statistical methods for computer algorithm comparisons. Stat Methods Med Res 2015;24:68–106.

[48] Mohamed ASR, Hansen C, Weygand J, Ding Y, Frank SJ, Rosenthal DI, et al. Prospective analysis of in vivo landmark point-based MRI geometric distortion in head and neck cancer patients scanned in immobilized radiation treatment position: Results of a prospective quality assurance protocol. Clin Transl Radiat Oncol 2017;7:13–9.

[49] Carr HY. Steady-state free precession in nuclear magnetic resonance. Phys Rev 1958;112:1693–701.

[50] Schleffler K, Lehnhardt S. Principles and applications of balanced SSFP techniques. Eur Radiol 2003;13:2409–18.

[51] Lawrence LSP, Chan RW, Chen H, Keller B, Stewart J, Ruschin M, et al. Accuracy and precision of apparent diffusion coefficient measurements on a 1.5 T MR-Linac in central nervous system tumour patients. Radiother Oncol 2021;164:155–62.

[52] Oka K, Yakushiji T, Sato H, Yorimitsu S, Hayashida Y, Yamashita Y, et al. Ability of diffusion-weighted imaging for the differential diagnosis between chronic expanding hematomas and malignant soft tissue tumors. J Magn Reson Imaging 2008;28:1195–200.

[53] Oka K, Yakushiji T, Sato H, Fujimoto T, Hirai T, Yamashita Y, et al. Usefulness of diffusion-weighted imaging for differentiating between desmoid tumors and malignant soft tissue tumors. J Magn Reson Imaging 2011;33:189–93.

[54] Razek A, Nada N, Ghaniem M, Elkhamary S. Assessment of soft tissue tumours of the extremities with diffusion echoplanar MR imaging. Radiol Medica 2012;117: 96–101.

[55] Gao Y, Han F, Zhou Z, Cao M, Kaprealian T, Kamrava M, et al. Distortion-free diffusion MRI using an MRI-guided tri-cobalt 60 radiotherapy system: Sequence verification and preliminary clinical experience. Med Phys 2017;44:5357–66.

[56] Hennig J, Nauerth A, Friedburg H. RARE imaging - A fast imaging method for clinical MR. Magn Reson Med 1986;3:823–33.

[57] Hirata K, Nakaura T, Okuaki T, Kidoh M, Oda S, Utsunomiya D, et al. Comparison of the image quality of turbo spin echo- and echo-planar diffusion-weighted images of the oral cavity. Medicine 2018; 97:e0447.

[58] Mori N, Mugikura S, Miyashita M, Mori Y, Maekawa Y, Nagasaka T, et al. Turbo spin-echo diffusion-weighted imaging compared with single-shot echo-planar diffusion-weighted imaging: image quality and diagnostic performance when differentiating between ductal carcinoma in situ and invasive ductal carcinoma. Magn Reson Med Sci 2021;1:60–8.

[59] Nardini M, Capotosti A, Mazzoni LN, Cusumano D, Boldrini L, Chiloiro G, et al. Tuning the optimal diffusion-weighted MRI parameters on a 0.35-T MR-Linac for clinical implementation: A phantom study. Front Oncol 2022;12:867792.

[60] Chizhik V, Frolov V, Kupryanov P, Tyutyukin K. Reduction of effect of concomitant gradients in low magnetic field MRI via optimization of gradient magnetic system. Appl Magn Reson 2017;48:687–98.

[61] Kooreman ES, Van Houdt PJ, Nowee ME, Van Pelt VWJ, Tijssen RHN, Paulson ES, et al. Feasibility and accuracy of quantitative imaging on a 1.5 T MR-linear accelerator. Radiother Oncol 2019;133:156–62.

[62] Thorwarth D, Ege M, Nachbar M, Mönnich D, Gani C, Zips D, et al. Quantitative magnetic resonance imaging on hybrid magnetic resonance linear accelerators: Perspective on technical and clinical validation. Phys Imaging Radiat Oncol 2020: 1669–73.

[63] Habrich J, Boeke S, Nachbar M, Nikolaou K, Schick F, Gani C, et al. Repeatability of diffusion-weighted magnetic resonance imaging in head and neck cancer at a 1.5 T MR-Linac. Radiother Oncol 2022;174:141–218.

[64] McDonald BA, Vedam S, Yang J, Wang J, Castillo P, Lee B, et al. Initial feasibility and clinical implementation of daily MR-guided adaptive head and neck cancer radiation therapy on a 1.5 T MR-linac system: Prospective R-IDEAL 2a/2b systematic clinical evaluation of technical innovation. Int J Radiat Oncol Biol Phys 2021;109:1606–18.

[65] Weygand J, Fuller CD, Ibbott GS, Mohamed ASR, Ding Y, Yang J, et al. Spatial precision in magnetic resonance imaging–guided radiation therapy: The role of geometric distortion. Int J Radiat Oncol Biol Phys 2016;95:1304–16.

[66] Michoux NF, Ceranka JW, Vandemeulebroucke J, Peeters F, Lu P, Absil J, et al. Repeatability and reproducibility of ADC measurements: A prospective multicenter whole-body-MRI study. Eur Radiol 2021;31:4514–27.

[67] Schenck F. The role of magnetic susceptibility in magnetic resonance imaging: MRI magnetic compatibility of the first and second kinds. Med Phys 1996;23:815–50.

[68] Weygand J, Carter SE, Salzillo TC, Moussalli M, Dai B, Dutta P, et al. Can an organoid recapitulate the metabolome of its parent tissue: A pilot NMR study. J Cancer Prev Curr Res 2017;7:00307.

[69] Wachowicz K, Stanescu T, Thomas SD, Fallone BG. Implications of tissue magnetic susceptibility-related distortion on the rotating magnet in an MR-linac design. Med Phys 2010;37:1714–21.

[70] Goelman G, Liu S, Fleysher R, Fleysher L, Grossman RI, Gonen O. Chemical-shift artifact reduction in hadamard-encoded MR spectroscopic imaging at high (3T and 7T) magnetic fields. Magn Reson Med 2007;58:167–73.

[71] Begnoche JP, Schilling KG, Boyd BD, Cai LY, Taylor WD, Landman BA. EPI susceptibility correction introduces significant differences far from local areas of high distortion. Magn Reson Imag 2022;92:1–9.

[72] Le Bihan D, Breton E, Lallemand D, Aubin ML, Vignaud J, Laval-Jeantet M. Separation of diffusion and perfusion in intravoxel incoherent motion MR imaging. Radiology 1988;168:497–505.

[73] Iima M, Le Bihan D. Clinical intravoxel incoherent motion and diffusion MR imaging: Past, present, and future. Radiology 2016;278:13–32.

[74] Padhani AR, Liu G, Mu-Koh D, Chenevert TL, Thoeny HC, Takahara T, et al. Diffusion-weighted magnetic resonance imaging as a cancer biomarker: Consensus and recommendations. Neoplasia 2009;11:102–25.

[75] Kooreman ES, Van Houdt PJ, Keesman R, Pos FJ, Van Pelt VMJ, Nowee ME, et al. ADC measurements on the Unity MR-linac – A recommendation on behalf of the Elekta Unity MR-linac consortium. Radiother Oncol 2020;153:106–13.

[76] Palacios EM, Martin AJ, Boss MA, Ezekiel F, Chang YS, Yuy EL, et al. Toward precision and reproducibility of diffusion tensor imaging: A multicenter diffusion phantom and traveling volunteer study. AJNR Am J Neuroradiol 2017;38:537–45.

[77] Huisman TAGM, Loenneker T, Barta G, Bellemann ME, Hennig J, Fischer JE, et al. Quantitative diffusion tensor MR imaging of the brain: field strength related variance of apparent diffusion coefficient (ADC) and fractional anisotropy (FA) scalars. Eur Radiol 2006;16:1651–8.

[78] Ogura A, Tamura T, Ozaki M, Doi T, Fujimoto K, Miyati T, et al. Apparent diffusion coefficient value is not dependent on magnetic resonance systems and field strength under fixed imaging parameters in brain. J Comput Assist Tomogr 2015; 39:760-765.